JOURNAL OF MATERIALS SCIENCE 32 (1997) 369–374

Extended X-ray absorption fine structure (EXAFS) study of secondary phases in Yb_2O_3-doped Si_3N_4 ceramics

P. KIZLER*, H. J. KLEEBE††, F. ALDINGER, M. RÜHLE
Max-Planck-Institut für Metallforschung, Institut für Werkstoffwissenschaft, Seestraße 92, D-70174 Stuttgart, Germany

Liquid-phase sintered Si_3N_4 doped with Yb_2O_3 as a sintering aid was characterized by both transmission electron microscopy and extended X-ray absorption fine structure (EXAFS) measurements. Structural information about the secondary phases was obtained with an emphasis being placed on the evaluation of EXAFS data. Two Si_3N_4 samples were processed which contained either 5 vol% or 10 vol% Yb_2O_3 as sintering additive. After sintering, only an amorphous secondary phase was observed in the material doped with 5 vol% Yb_2O_3. The material with the higher Yb_2O_3 volume fraction underwent a further heat treatment after the densification, in order to crystallize pockets of the secondary phase. This heat treatment resulted in the formation of $Yb_2Si_2O_7$ at multi-grain junctions, with however, amorphous phases remaining along the grain and phase boundaries. The EXAFS data obtained from the two doped Si_3N_4 materials were compared with reference spectra obtained on pure Yb_2O_3 and synthetic $Yb_2Si_2O_7$. No residual Yb_2O_3 was determined in the doped Si_3N_4 materials, independent of the Yb_2O_3 volume fraction. Compared to synthetic $Yb_2Si_2O_7$, the secondary phase formed in the 10 vol% Yb_2O_3 containing material showed only subtle changes in the EXAFS data. A clear distinction between purely amorphous and a combination of crystalline plus amorphous Yb secondary phases was possible, when both doped Si_3N_4 materials were compared. However, no distinction between the glass phase present at triple junctions and the amorphous residue along grain/phase boundaries was feasible, since a full numerical data evaluation could not be performed.

1. Introduction

In the early sixties, Deely *et al.* were the first to demonstrate that the complete densification of Si_3N_4-powder compacts during pressureless sintering could only be achieved with the aid of sintering additives [1]. This is due to the highly covalent bonding characteristics of the Si_3N_4 structure which results in a low self-diffusivity of α- and β-Si_3N_4 even at 1400 °C [2]. Depending on both the sintering aid composition and the processing parameters either amorphous or a combination of crystalline and amorphous secondary phases can form upon cooling. A post-sintering heat-treatment induces crystallization of the amorphous secondary phase in triple-grain regions [3–5], which greatly reduces the volume fraction of residual glass. However, complete crystallization of the glass phase cannot be achieved, because thin intergranular films along two-grain junctions remain non-crystalline [6, 7]. Such intergranular films are observed between all but low-angle grain boundaries in Si_3N_4 ceramics and can range in width from 0.5–4 nm [8]. It should be noted that a distinction between grain and phase boundaries is made, with phase boundaries (interfaces between different adjacent grains, e.g., $Si_3N_4/Yb_2Si_2O_7$) commonly being wider [8]. The residual glass phase, such as intergranular films, are generally assumed to consist mainly of SiO_2 (from the surface of the Si_3N_4 grains) with dissolved cations, that stem from the utilized sintering aids. More recently, anions have also been reported to segregate at interfaces and hence change both glass structure and chemistry [9, 10]. With respect to nitrogen solubility it is known that N-incorporation into rare earth (RE) glasses changes the bulk glass properties. A higher N-volume fraction yields a higher density, viscosity, Young's modulus, and higher transition temperature of the glass [11, 12]. Apart from these results reported in the literature, little is known about the structure and chemistry of such RE-oxinitride glasses, which form upon densification within the materials. However, the detrimental effect of the presence of such residual amorphous phases, formed in liquid-phase sintered Si_3N_4 ceramics, on high-temperature properties is well established [13]. Therefore, a detailed

* Current address: DESY LIASYLAB, Notkestraße 85, D-22603 Hamburg, Germany
†† Current address: Universität Bayreuth, Institut für Materialforschung, Ludwig-Thoma-Straße 36b, D-95440 Bayreuth, Germany

0022–2461

characterization of the structure and chemistry of such glasses is required, in order to better understand the interaction of glass and bulk material properties.

The secondary phases present in Si_3N_4 ceramics doped with Yb_2O_3 have been investigated by a combination of transmission electron microscopy (TEM), high-resolution and analytical electron microscopy (HREM and AEM), and the results of these investigations have been reported elsewhere [14]. The observed secondary phases consisted of both amorphous and crystalline compounds, depending on the volume content of the sintering aid and subsequent heat treatment. With an increasing amount of Yb_2O_3 addition, the volume fraction of the amorphous phase versus its crystalline counterpart decreases. Information on the composition of the Yb–Si–O phase and a resolution of the question as to whether the secondary phases are predominantly crystalline or amorphous are difficult to obtain without the destruction of the investigated sample, i.e., during TEM-foil preparation. Therefore, it is worthwhile to consider the application of a more direct, non-destructive structural probe, the extended X-ray absorption fine structure (EXAFS) spectroscopy. The main advantage of using this method as a structural probe is that it only probes the local short range order existing around the X-ray absorbing atoms. The low absorption coefficient of Si and N for X-rays at the energy of the Yb-L_3 absorption edge offers favourable conditions for such experiments, as has already been demonstrated for different grain boundary phases in Si_3N_4 ceramics doped with yttria and ceria (Y-K- and Ce-L_3 absorption edges) [15].

In this paper we report a first attempt to combine both TEM and EXAFS studies in order to gather information on the structure of secondary phases formatted in Si_3N_4 doped with Yb_2O_3. The motivation for this work was to answer the question as to whether or not it is possible to extract information about the local structure of the glass phase present at grain boundaries and if possible to distinguish between the bulk glass structure and the amorphous structure within the intergranular films.

2. Experimental procedure

2.1. Materials and TEM characterization

The Si_3N_4 samples were processed via liquid-phase sintering at 1800 °C for 2 h of the cold isostatically pressed powder compacts under a 0.1 MPa N_2-pressure. The sintering aid for complete densification consisted of 5 vol % or 10 vol % Yb_2O_3 with the extra addition of 0.5 vol % Al_2O_3 for improved sinterability. After sintering, the material with the higher Yb_2O_3-volume fraction underwent a further heat treatment for 12 h at 1250 °C under a 0.1 MPa N_2-pressure in order to crystallize secondary phase pockets, i.e., to form $Yb_2Si_2O_7$.

TEM-foil preparation was performed using standard techniques involving mechanical grinding, dimpling, ion thinning to perforation, and a light carbon coating to minimize electrostatic charging effects in the electron microscope. The microstructural characterization of both materials was performed by means of conventional transmission electron microscopy (CTEM) utilizing a Jeol 2000 FX microscope, fitted with an energy dispersive spectroscopy ultra-thin window Ge-detector (EDX) system. Identification of the crystalline secondary phases formed upon heat treatment (10 vol % Yb_2O_3 addition) was performed by both X-ray diffraction (XRD) and electron diffraction in addition to EDX. Intergranular films were characterized by the HREM imaging technique, which was performed using a Jeol 4000 EX microscope operating at 400 kV with a point resolution of 0.18 nm.

2.2. X-ray absorption and EXAFS measurements

The X-ray absorption (XAS) measurements were performed in transmission mode at liquid nitrogen temperature at the station EXAFS II (Yb-L_3 edge, 8944 eV) at the Hamburger Synchrotronstrahlungslabor HASYLAB. HASYLAB utilizes synchrotron radiation generated by the storage ring DORIS at the Deutsches Elektronen-Synchrotron DESY. The station operates a double crystal monochromator, which is equipped with a Si-$\{1\,1\,1\}$ crystal and achieves an energy resolution of $\Delta E < 1$ eV. The intensities before and after the samples were detected with nitrogen filled ionization chambers. Higher order diffraction in the monochromator was suppressed by detuning the monochromator with a feedback system [16] and by the intensity cutoff due to a focussing gold-coated mirror in the beam path. The energy position of the Yb-K edge ($E = 61332$ eV) is too high to be accessed by typical experimental stations, therefore, the Yb-L_3 absorption edge had to be used.

EXAFS can be considered as the modulation of the photoabsorption cross section due to the interference between the de Broglie wave of the ejected photoelectron with that which is backscattered by the surrounding atoms [17, 18]. The main advantage of utilizing this effect as a structural probe is its selectivity to the neighbourhood around the X-ray absorbing species.

2.2.1. Data reduction

Data reduction followed a standard procedure as reported elsewhere [19] of pre-edge and post-edge background removal, edge normalization, extraction of the EXAFS signal $\chi(k)$ and Fourier transformation of $\chi(k)$. The pre-edge background removal was performed by applying the usual Victoreen-fit to the pre-edge data and extrapolating it into the post-edge region under the boundary condition of leaving over an absorption coefficient in agreement with the calculations of Cromer and Liberman [20]. The post-edge background in the EXAFS region was generated by a fit of 4th order polynomials. Such polynomials are "stiff" enough to prevent the post-edge background curve from taking part in any of the structure-related data oscillations. These two conditions (agreement of absorption coefficient with calculations + stiff polynomials) remove two important sources of possible error in the numerical data interpretation. The energy

scale was converted to the (k) scale using Equation 1:

$$k = \frac{1}{h}(\sqrt{2}m(E - E_0))^{1/2} \quad (1)$$

where E_0 is the energy threshold of the absorption edge. The normalized EXAFS $\chi(k)$ was obtained by subtracting the smooth post-edge background, μ_0, from the measured absorption, $\mu(k)$, and dividing again by the smooth absorption $\mu_0(k)$ as given in Equation 2:

$$\chi(k) = \frac{\mu(k) - \mu_0(k)}{\mu_0(k)} \quad (2)$$

3. Results

3.1. TEM observations

The transmission electron microscopy (TEM) studies on the two different Si_3N_4 materials investigated only showed marked differences in the secondary phases observed. The 5 vol % Yb_2O_3 doped Si_3N_4 exclusively showed an amorphous phase present at triple pockets and along grain boundaries. The amorphous nature of the residue, observed at triple junctions, was confirmed by selected area electron diffraction (SAD). The amorphous nature of the intergranular films was verified by HREM imaging [21]. Fig. 1 depicts a typical multi-grain junction solely filled with the amorphous phase, which was also found along two-grain junctions. It should be noted that no crystalline phases other than the Si_3N_4 matrix grains were observed in this low-doped material. However, since the 10 vol % Yb_2O_3-containing sample underwent a post-sintering heat treatment, crystallization of secondary phases was initiated. A more detailed characterization of the crystallization behaviour of these materials is reported elsewhere [14, 22]. X-ray diffraction (XRD) and SAD studies in combination with chemical analysis (EDX) verified the presence of $Yb_2Si_2O_7$ within the triple pockets upon heat treatment (compare Fig. 2). Owing to the crystallization of the large multi-grain pockets, the residual glass volume fraction was greatly reduced. However, apart from these crystalline secondary phases observed, amorphous intergranular films were still present at Si_3N_4/Si_3N_4 grain boundaries, as is shown in Fig. 3, as well as at phase boundaries $Si_3N_4/Yb_2Si_2O_7$, as depicted in Fig. 2.

Summarizing the TEM results it can be stated that the Si_3N_4 sample with the lower Yb_2O_3 content only revealed residual glass. Assuming that the glass structure (and chemistry) is different at grain boundaries and within triple pockets, one has to distinguish

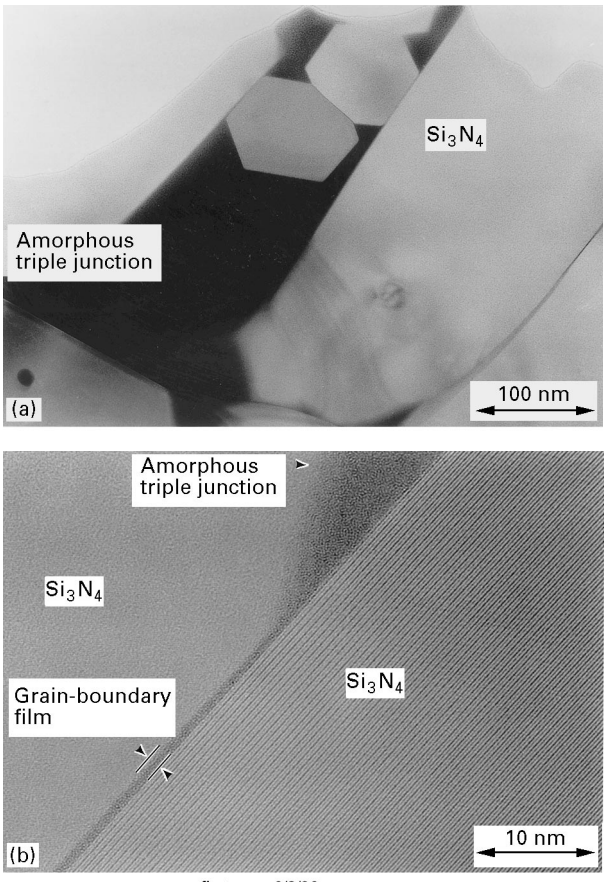

Figure 1 Low magnification TEM micrograph of the as-sintered Si_3N_4 material doped with 5 vol % Yb_2O_3. Note that only an amorphous secondary phase is present at the large multi-grain junctions shown in (a) as well as along two-grain junctions depicted in (b).

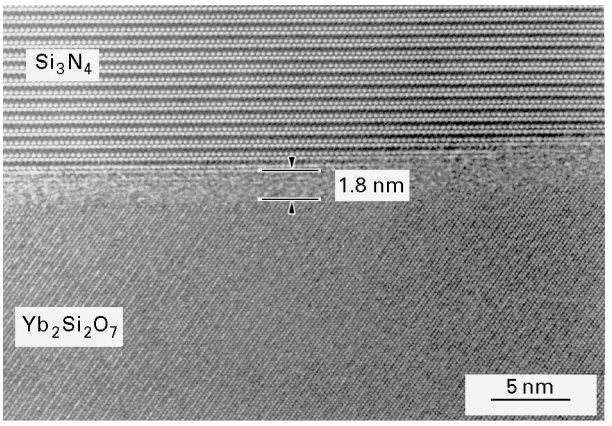

Figure 2 HREM micrograph of a phase boundary in the annealed Si_3N_4 material containing 10 vol % Yb_2O_3. SAD studies in conjunction with EDX analysis identified $Yb_2Si_2O_7$ as the secondary crystalline phase. The intergranular film thickness was evaluated to 1.8 nm. Note that the film thickness of the phase boundary is wider than of the grain boundary (compare Figure 3).

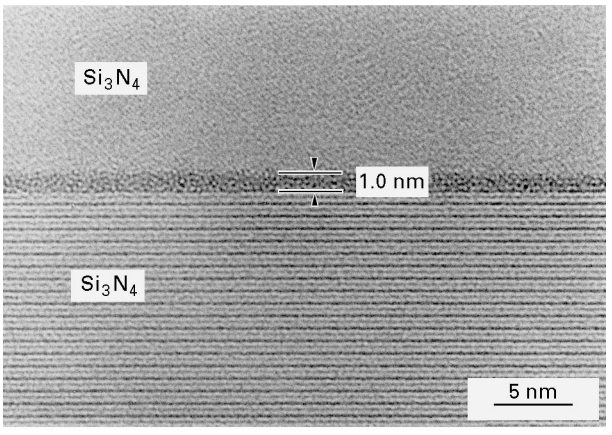

Figure 3 HREM micrograph of a grain boundary in the as-sintered Si_3N_4 material containing 5 vol % Yb_2O_3. The thickness of the amorphous intergranular film within this material was evaluated to 1.0 nm (using β-Si_3N_4 lattice fringes as internal reference).

TABLE I Amorphous and crystalline phases in the Yb_2O_3 doped Si_3N_4 materials. Note that the major difference within the two materials is the crystallinity of the triple pockets

Material	Intergranular films		Triple pockets
	Grain boundaries	Phase boundaries	
5 vol % Yb_2O_3 as-sintered	Amorphous	Amorphous	Amorphous
10 vol % Yb_2O_3 annealed	Amorphous	Amorphous	$Yb_2Si_2O_7$

between interfacial glass and any amorphous residue formed at multi-grain pockets. This assumption is mainly based on the idea that glass formation is mostly constrained at grain boundaries (with a width of about 1.0 nm) while the formation of residual glass pockets leaves a higher degree of freedom (with respect to the positioning of structural units, e.g., SiO_4-tetrahedra). The Si_3N_4 sample containing the higher Yb_2O_3 volume fraction also shows two distinct secondary phases, both of which contain Yb, (i) an amorphous intergranular film (constrained interfacial glass) and (ii) the crystalline $Yb_2Si_2O_7$ phase (compare also Table 1). The EXAFS study was performed in addition to TEM observations, in order to answer the following unresolved questions: (i) is a distinction between amorphous and crystalline secondary phases feasible and (ii) can indeed a difference between interfacial glass and residual glass pockets be found?

3.2. EXAFS measurements

In Fig. 4 we present the raw data collected from the samples and in Fig. 5 the $\chi(k)$ curves, as derived from the raw data, are displayed. On the basis of the single scattering approximation [17, 18], the observed EXAFS $\chi(k)$ may be described by Equation 3:

$$\chi(k) = \frac{-1}{k} \sum_j A_j \sin\left[2r_j k + \phi_j(k)\right] \quad (3)$$

having oscillatory terms with frequencies $[2r_j k + \phi_j(k)]$ and amplitude terms A_j given by Equation 4:

$$A_j = \frac{N_j}{r_j^2} f(\pi, k) \exp\left\{\frac{-2r_j}{\lambda}\right\} \exp\left(-2\sigma_j^2 k^2\right) \quad (4)$$

The parameters on the right hand side of Equations 3 and 4 may be classified as (i) scattering parameters, which include the phase shift $\phi_j(k)$, the backscattering amplitude $f_j(\pi, k)$ and electron mean free path λ, and (ii) structural parameters, which include the coordination number N_j, bond distance r_j, and Debye–Waller factor σ_j. The phase shift $\phi_j(k)$ is composed of the central atom phase shift $\phi_c(k)$ and the backscattering phase shift $\phi_b(k)$ as given by Equation 5:

$$\phi_j(k) = 2\phi_c(k) + \phi_b(k) \quad (5)$$

for each pair of atomic species, respectively. The summation is over all coordination shells j participating in the EXAFS event. For the conclusions later on it should be borne in mind that for different samples differences in the amplitude of $\chi(k)$ can be caused by differences in the coordination number N_j as well as by differences in the Debye–Waller term σ_j. The other parameters are identical for the present samples. The Debye–Waller term consists of a thermal and a structural term, as given in Equation 6:

$$\sigma^2_{\text{total}} = \sigma^2_{\text{thermal disorder}} + \sigma^2_{\text{structural disorder}} \quad (6)$$

The thermal disorder is minimized by cooling the samples to liquid nitrogen temperature and thus only the structural disorder remains as a subject of consideration. The scattering parameters of Equations 3 and 4 can be empirically derived from reference compounds. Such data being available, a numerically precise data evaluation process would employ a fit algorithm varying N_j, r_j and σ_j in the EXAFS Equation 3 until the best agreement between calculated and experimental $\chi(k)$ is achieved. In the present case Yb has simultaneously Si and O neighbours, and at the border to a Si_3N_4 grain even N neighbours. The backscattering amplitudes of Si and O differ by a factor of approximately 2, and also the backscattering phase shifts are different. Unfortunately, this

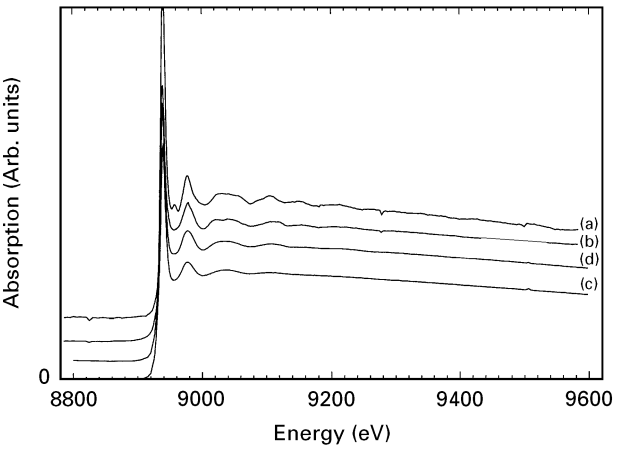

Figure 4 Yb-L_3 X-ray absorption data of (a) Yb_2O_3, (b) $Yb_2Si_2O_7$ and Si_3N_4 doped with (c) 5 and (d) 10 vol % Yb_2O_3. The pre-edge absorption was already subtracted.

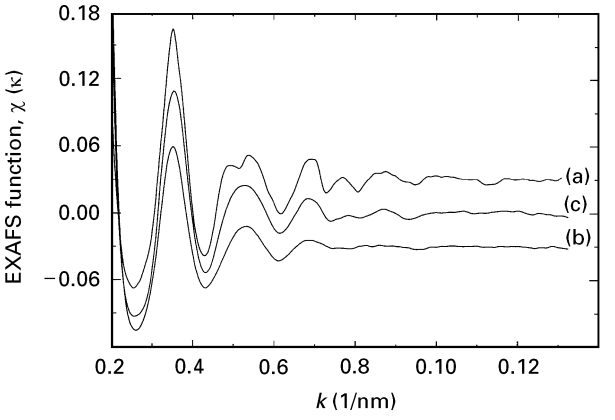

Figure 5 EXAFS functions as extracted from the absorption data of Fig. 4: $\chi(k)$ data of (a) $Yb_2Si_2O_7$ and Si_3N_4 doped with (b) 5 and (c) 10 vol % Yb_2O_3.

makes a full numerical data evaluation impossible. Moreover, as observed during TEM investigations, Yb can co-exist simultaneously in a crystalline as well as in an amorphous substructure. Therefore, there would be far too many free parameters for an EXAFS fit. Hence, for the present study one has to exclude a full numerical data evaluation and instead interpret the frequency analysis of the $\chi(k)$ spectrum in terms of the Fourier transform, which yields a radial structure function $F(r)$ in real space, as given in Equation 7:

$$F(r) = \frac{1}{2\pi} \int_{\kappa_{min}}^{\kappa_{max}} W(k)\, k^{n}\, \chi(k)\, \exp^{(2\pi i r)}\, dk \qquad (7)$$

where $W(k)$ is a Kaiser–Bessel window function which is utilized in order to minimize truncation effects in the Fourier transformation [23], which is described analytically in Equation 8:

$$W(k) = I_0(\beta(1 - [(k - k^1)/r]^2))^{1/2}/I_0(\beta) \qquad (8)$$

with $k' = (k_{max} + k_{min})/2$, $\tau = (k_{max} - k_{min})/2$ and I_0 being the modified Bessel function of first type and zeroth order. The peak radii of the Fourier transform differ from the true atomic distances because of the phase shift $\phi_j(k)$ (see Equation 3), nevertheless, the Fourier transform provides a true image of the short-range order around the absorbing atomic species.

3.2.1. EXAFS of Yb-containing phases

Two reference materials were utilized, pure Yb_2O_3 and synthetic $Yb_2Si_2O_7$, and the EXAFS data obtained on these compounds were compared to the two Yb_2O_3-doped Si_3N_4 materials under investigation. In Fig. 6, the Fourier transforms of the EXAFS data depicted in Fig. 5, calculated for the same k range ($k_{min} = 0.222\ nm^{-1}$, $k_{max} = 1.35\ nm^{-1}$), are displayed. For the window function $W(k)$ a k^1 weighting together with the parameter $\beta = 4$ was used because this value provides a good compromise between resolution in r space and intensity of side lobes [24].

The first peak around 0.18 nm is attributed to the O or Si/O shell of atoms around the Yb atom. In pure Yb_2O_3 each Yb atom has six oxygen bonds, composed of two with $r = 0.222$ nm, 0.224 nm and 0.231 nm, respectively. In $Yb_2Si_2O_7$, the closest Yb-neighbour distances are two O at 0.222 nm, two at 0.221 nm and two at 0.228 nm, followed by a slightly larger Yb–Si distance. The second peak around 0.3 nm solely belongs to Yb–Yb bonds (in $Yb_2Si_2O_7$ the Yb–Yb distance is 0.33 nm), because within the major k range, the strong backscattering amplitude of Yb dominates the weak scattering power of O [25, 26]. Although the Yb–O distances and the coordination numbers of pure Yb_2O_3 and synthetic $Yb_2Si_2O_7$ are almost identical, the Fourier peak for $Yb_2Si_2O_7$ is a little smaller. This is caused by the Si atoms, whose electron backscattering amplitude is roughly two times as strong as the one of oxygen. The difference in backscattering phase shifts between O and Si atoms amounts to approximately 2.5 rad [25, 26] throughout the typical k range. Therefore, electron waves scattered from Si destructively interfere with the waves backscattered from oxygen thus diminishing the Fourier peak. On the other hand, the loss in peak amplitude is not too severe. Therefore, despite the discussed complexity of scattering events, as a first approach, the data can be regarded as if they would belong to a pure oxygen bond.

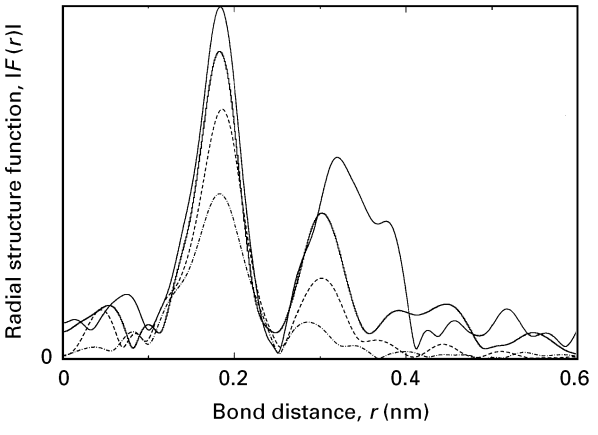

Figure 6 Fourier transformed $\chi(k)$ data (see also Fig. 5) of (—) Yb_2O_3, (∼∼) $Yb_2Si_2O_7$ and Si_3N_4 doped with (–·–) 5 and (– – –) 10 vol % Yb_2O_3.

4. Discussion

From the Fourier transformed data shown in Fig. 6 one can recognize that the short range order around Yb within the 10 vol % Yb_2O_3 doped Si_3N_4 sample belongs to the $Yb_2Si_2O_7$ type, although it is slightly disturbed. This means that Yb_2O_3 has undergone a chemical reaction which has converted it to $Yb_2Si_2O_7$. This result is consistent with XRD measurements as well as with TEM observations (electron diffraction). A loss in the peak height of the Fourier transform can either be caused by a loss in coordination number or by an increase in structural disorder σ_j (see also Equation 6). In a dense solid, a loss in coordination number is quite unlikely, therefore, an increase of σ_j remains for consideration. In the case of the 5 vol % Yb_2O_3 doped sample, the short range order is even more disordered than in the 10 vol % Yb_2O_3 containing one. This is also consistent with the TEM results reported earlier. For the low ytterbia content sample, the sintering additive is mainly present as interfacial glass and at smaller triple pockets filled with glass, whereas for the higher Yb_2O_3-volume fraction sample crystalline phases predominate.

Since EXAFS is a non-destructive but integral analytical tool, both amorphous secondary phases, interfacial glass and glass pockets, were analysed with respect to the Si_3N_4 material containing the 5 vol % Yb_2O_3 addition (compare also Table 1). Therefore, no distinction between phases present at triple pockets or along grain boundaries could be readily made. For the higher volume fraction of sintering aid, however, the residual amorphous phase (interfacial glass) in addition to the crystalline secondary phase $Yb_2Si_2O_7$ contribute to the EXAFS signal. Hence, the difference spectrum between synthetic $Yb_2Si_2O_7$ and 10 vol % Yb_2O_3-containing Si_3N_4 should in principal only contain information on the interfacial glass. If, in

addition, a variation between this difference spectrum and the 5 vol % EXAFS data could be determined, the aforementioned assumption of different glass structures at the triple junctions and at grain boundaries would be verified. Unfortunately however, as mentioned above, in addition to the complex Si_3N_4 microstructure, a full EXAFS data evaluation could not be performed, which made it impossible to experimentally distinguish between interfacial glass and amorphous residue present at triple pockets.

5. Conclusions

The present study has shown that EXAFS spectroscopy can be a helpful non-destructive tool to characterize secondary phases in ceramic materials. As stated earlier, the combination of both TEM and EXAFS techniques was chosen in order to yield information on the structure of secondary phases formed in Yb_2O_3-fluxed Si_3N_4. Unfortunately, the question as to whether it is possible to extract information about the interfacial glass structure has to be answered with a "no". The complexity of the Si_3N_4 system prevents a full data evaluation and hence leaves such questions unresolved. However, it should be borne in mind that the results presented in this paper clearly indicate the possibility of distinguishing between crystalline and amorphous Yb-secondary phases. Moreover, the presence of residual Yb_2O_3 (after densification) could uneqivocally be excluded for both materials. Thus, the results obtained by EXAFS are fully consistent with the TEM observations. It is concluded that the combination EXAFS and TEM techniques has proven to be a valuable tool with respect to detailed materials characterization.

Acknowledgements

Prof. M. J. Hoffmann and Dr. E. Hampp are greatly acknowledged for providing the Yb_2O_3-containing Si_3N_4 materials.

References

1. G. G. DEELY, G. M. HERBERT and N. C. MOORE, *Powder Metall.* **8** (1961) 145.
2. R. RAJ and M. F. ASHBY, *Metall. Trans.* **2A** (1971) 1113.
3. L. K. L. FALK and G. L. DUNLOP, *J. Mater. Sci.* **22** (1987) 4369.
4. D. A. BONNELL, T. -Y. TIEN and M. RÜHLE, *J. Amer. Ceram. Soc.* **70** (1987) 460.
5. M. K. CINIBULK, G. THOMAS and S. M. JOHNSON, *ibid* **73** (1990) 1606.
6. H.-J. KLEEBE, M. K. CINIBULK, I. TANAKA, J. BRULEY, R. M. CANNON, D. R. CLARKE and M. RÜHLE, *Mat. Res. Soc. Symp. Proc.* **287** (1993) 65.
7. H.-J. KLEEBE, M. K. CINIBULK and M. RÜHLE, *J. Amer. Ceram. Soc.* **76** (1993) 1969.
8. H.-J. KLEEBE and M. K. CINIBULK, *J. Mater. Sci. Lett.* **12** (1993) 70.
9. I. TANAKA, K. IGASHIRA, H.-J. KLEEBE and M. RÜHLE, *J. Amer. Ceram. Soc.* **77** (1994) 275.
10. G. PEZZOTTI, K. MATSUCHITA, H. -J. KLEEBE, Y. OKAMOTO and T. NISHIDA, *Acta Metall. Mater.* **43** (1995) 4357.
11. H.-O. MULFINGER, *J. Amer. Ceram. Soc.* **49** (1966) 462.
12. S. H. RISBUD, *Physics and Chemistry of Glasses* **22** (1981) 168.
13. A. TSUGE, K. NISHIDA and M. KOMATSU, *J. Amer Ceram. Soc.* **58** (1975) 323.
14. J. S. VETRANO, H.-J. KLEEBE, E. HAMPP, M. S. HOFFMANN, R. M. CANNON and M. RÜHLE, *J. Mater. Sci.* **28** (1992) 3529.
15. N. KAMIJO, H. KAGEYAMA and T. YAMAMOTO, *Physica B* **158** (1989) 513.
16. A. KROLZIG, G. MATERLIK, M. SWARS and J. ZEGENHAGEN, *Nucl. Instr. Meth.* **219** (1984) 430.
17. D. C. KONINGSBERGER and R. PRINS, "X-Ray Absorption, Principles, Applications and Techniques" (John Wiley, New York, 1988).
18. B. K. TEO, "EXAFS, Basic Principles and Data Analysis" (Springer, Berlin, 1986).
19. R. FRAHM, R. HAENSEL and P. RABE, *J. Phys. F* **14** (1984) 1029.
20. D. T. CROMER and D. A. LIBERMAN, *J. Chem. Phys.* **53** (1970) 1891.
21. M. K. CINIBULK, H.-J. KLEEBE and M. RÜHLE, *J. Amer. Ceram. Soc.* **76** (1993) 426.
22. J. S. VETRANO, H.-J. KLEEBE, E. HAMPP, M. S. HOFFMANN and M. RÜHLE, *J. Mater. Sci. Lett.* **11** (1992) 1249.
23. F. F. KUO and J. F. KAISER, "System Analysis by Digital Computer" (Wiley, New York, 1966).
24. T. BUTZ, A. VASQUEZ and A. LERF, *J. Phys. C* **12** (1979) 4509.
25. B. K. TEO and P. A. LEE, *J. Amer. Chem. Soc.* **101** (1979) 2815.
26. A. G. McKALE, B. W. VEAL, A. P. PAULIKAS, S. K. CHAN and G. S. KNAPP, *ibid* **110** (1988) 3763.

Received 2 March
and accepted 2 July 1996